Journal of Analytical and Applied Pyrolysis 156 (2021) 105165

Contents lists available at ScienceDirect

Journal of Analytical and Applied Pyrolysis

journal homepage: www.elsevier.com/locate/jaap

Biomass fast pyrolysis in an innovative gas-solid vortex reactor: Experimental proof of concept

Manuel Nunez Manzano [a], Arturo Gonzalez Quiroga [b], Patrice Perreault [c], Sepehr Madanikashani [a,d], Laurien A. Vandewalle [a], Guy B. Marin [a], Geraldine J. Heynderickx [a], Kevin M. Van Geem [a,*]

[a] Ghent University, Laboratory for Chemical Technology, Technologiepark 125, 9052, Gent, Belgium
[b] Universidad del Norte, UREMA Research Unit, Department of Mechanical Engineering, Barranquilla, Colombia
[c] University of Antwerp, Faculty of Science, Instituut Voor Milieu & Duurzame Ontwikkeling (IMDO), Campus Groenenborger. Gronenborgerlaan 171, 2020, Antwerpen, Belgium
[d] Université catholique de Louvain, Materials and Process Engineering (IMAP), Institute of Mechanics, Materials and Civil Engineering (iMMC), Place Sainte Barbe 2, B-1348 Louvain-la-Neuve, Belgium

ARTICLE INFO

Keywords:
Biomass
Pyrolysis
Gas-Solid Vortex Reactor
Process intensification

ABSTRACT

Biomass fast pyrolysis has been considered one of the best alternatives for the thermal conversion of biomass into bio-oil. This work introduces a new reactor technology for biomass fast pyrolysis, the Gas-Solid Vortex Reactor (GSVR), to obtain high bio-oil yields. The GSVR was designed to decrease the residence time of the pyrolysis vapors; thus, the secondary cracking reactions are reduced, to enhance the segregation of the char and the unreacted biomass and to improve the heat transfer rate. Biomass fast pyrolysis experiments have been carried out for the first time in a Gas-Solid Vortex Reactor (GSVR) at 773 K, using softwood (pine) and hardwood (poplar) as feedstock. Char yields as low as 10 wt. % in the GSVR were comparable to those reported for the same feedstocks processed in conventional fluidized bed reactors. The yields of non-condensable gases in the range of 15–17 wt. % were significantly lower than those reported for other commonly used biomass fast pyrolysis reactors. Two-dimensional gas chromatography (GC × GC) revealed noticeable differences at the molecular level between the bio-oils from the GSVR and bio-oils from other reactors. The aromatics in the pine bio-oil consist almost entirely (85 wt. %) of guaiacols. For poplar bio-oils no predominant group of aromatics was found, but phenolics, syringols, and catechols were the most pronounced. The experimental results highlight the advantages of the GSVR for biomass pyrolysis, reaching stable operation in around 60 s, removing the formed char selectively during operation, and enabling fast entrainment of pyrolysis vapors. Results indicate a great potential for increasing yield and selectivity towards guaiacols in softwood (e.g., pine) bio-oil. Likewise, decreasing pyrolysis temperature could increase the yield of guaiacols and syringols in hardwood (e.g., poplar) bio-oil.

1. Introduction

The high dependence on fossil resources for the production of chemicals and fuels, and the concerns about global warming are pushing the use of cleaner and renewable alternatives [1]. In this context, lignocellulosic biomass could be considered a reasonable option to replace the use of non-renewable resources, reducing CO_2 emissions [2–4]. Fast pyrolysis is one of the promising routes to convert biomass into valuable products because the process conditions can be optimized to maximize the yields of non-condensable gases, bio-oil and char [3,5,6].

Fast pyrolysis is the thermochemical degradation of organic matter under the absence of oxygen, at moderate temperatures (723−873 K) [3,

Abbreviations: CFB, Circulating Fluidized Bed; CWR, Cell Wall Residue; ESP, ElectroStatic Precipitator; FB, Fluidized Bed; FID, Flame Ionization Detector; GC×GC, Comprehensive two-dimensional Gas Chromatography; GC×GC-FID/TOF-MS, Comprehensive two-dimensional Gas Chromatography coupled with a Flame Ionization detector and a Time Of Flight Mass Spectrometer; GSVR, Gas Solid Vortex Reactor; Gu, Guaiacyl; HHV, Higher Heating Value; Hy, P-hydroxyphenyl; LCT, Laboratory for Chemical Technology; Py-GC/MS, Pyrolysis-gas chromatography-mass spectrometry; RGA, Refinery Gas Analyzer; SB, Spouted Bed; Sy, Syringyl; TCD, Thermal Conductivity Detector.

* Corresponding author.
E-mail address: Kevin.VanGeem@UGent.be (K.M. Van Geem).

https://doi.org/10.1016/j.jaap.2021.105165
Received 18 December 2020; Received in revised form 25 March 2021; Accepted 12 April 2021
Available online 15 April 2021

Nomenclature

f_i	Response factor of the component i.
A_i	Peak surface area of the component i.
$\dot{m}_i$	Mass flow rate of the component i (g/s).
Wt.	% Composition in weight percentage.

7]. The yields and properties of the pyrolysis products vary over several factors, including the type of feedstocks, pyrolysis processing conditions, and reactor technology [2,5,8–11]. The reactor features considered essential for fast pyrolysis are accurate temperature control, very high heat transfer rate, rapid char removal, and fast entrainment of the pyrolysis vapors [2,5,8,12–14]. Based on these requirements, fluidized bed (FB), circulating fluidized bed (CFB), and spouted bed (SB) reactors have been extensively used for biomass fast pyrolysis, due to their advantages such as efficient heat transfer and solid bed temperature stability [7,15]. However, there are appreciable limitations for these technologies such as the low solid bed density and the need for sufficiently low gas velocities to avoid solid entrainment [16]. The latter is a substantial limitation for fast pyrolysis because low gas velocities limit the heat transfer rates at particle scale due to the limited slip velocities. Thus, the search for new reactor technologies is an important research topic.

The reactor technology examined in the present work is the Gas-Solid Vortex Reactor (GSVR). In a GSVR, a rotating bed of particles is formed in a static cylindrical chamber through high-velocity gas injection via tangentially inclined inlet slots [17–19]. Momentum is transferred from the gas to the solid particles, causing them to rotate inside the chamber, thus generating a high centrifugal acceleration, up to two orders of magnitude higher than the Earth's gravitational acceleration. The radially-outward centrifugal force compensates the radially-inward drag force exerted by the gas that leaves the chamber via a central outlet. These operational conditions result in denser solids beds and higher gas-solid slip velocities compared with FBs, thus increasing heat and mass transfer rates [20,21]. Previously published studies [16,18,20,22–24] have proved that the gas-phase residence time in the GSVR is between 5 and 50 ms. These features match the desired characteristics for a fast pyrolysis reactor.

A GSVR demonstration unit for biomass fast pyrolysis has been built and tested at the Laboratory for Chemical Technology (LCT). Non-reactive experiments with pine particles and air have shown that the GSVR achieves a high centrifugal-to-drag force ratio for sustaining a rotating solids bed [18]. Additionally, cold-flow experiments with mixtures of biomass-derived char and biomass confirmed the effective retention of unconverted biomass and selective entrainment of char [25]. This offers a significant advantage over conventional FBs and other reactor technologies in which the formed char can further react due to its catalytic activity, potentially promoting the cracking of bio-oil components and leading to reduced liquid yields of up to 20 % [5,26].

In this work, for the first time fast pyrolysis experiments were performed in the GSVR, a milestone in the development of this technology. Detailed yields of the light gases and bio-oils obtained from fast pyrolysis of soft and hardwood, i.e., pine and poplar, are presented. The products were extensively characterized using comprehensive two-dimensional gas chromatography (GCxGC). The experiments are compared with those obtained in conventional FBs at similar operating conditions, proving the potential of the GSVR for pyrolysis processes.

2. Material and methods

2.1. Raw material

Two types of biomass were studied: pinewood, a softwood; and poplar, a hardwood. These materials have been grounded and sieved to a particle size in the 2.5–3.5 mm range and dried to a moisture content around 10 wt. %. Ultimate and proximate analysis were carried out in a Flash EA2000 (Interscience, Belgium) equipped with a thermal conductivity detector (TCD) detector and with a muffle furnace (Nabertherm LT 15/13) set to 848 K, respectively. The samples were oven-dried at 378 K for about 24 h to remove residual moisture. Table 1 summarizes the main characteristics of the raw biomasses.

Despite their similarities in elemental composition, there are notable differences between pine and poplar at the molecular level. Pinewood exhibits a high lignin (26.9–32.0 wt. %) and glucan (41.7–45.0 wt. %) content and low mannan (10.8–11.6 wt. %) and xylan (5.5–7.0) amounts. Poplar has a similar content of lignin (23.0–26.9 wt. %) and glucan (41.4–48.1 wt. %), a higher content of xylan (10.4–17.4 wt. %), and lower content of mannan (1.2–3.2 wt. %) than pinewood [13,28].

Lignin is the result of the polymerization of three different structural units: guaiacyl (Gu), p-hydroxyphenyl (Hy), and syringyl (Sy). The lining in softwood is predominantly composed of guaiacyl. The lignin in hardwood is composed of guaiacyl and syringyl [29,30]. Since the molecular composition of the lignocellulosic biomass has an essential effect on the composition of the produced bio-oil, the fractions of the different lignin structural units have been quantified according to the method described by Van Acker et al. [31]. Dry samples of biomass were subjected to a sequential extraction to obtain a purified Cell Wall Residue (CWR). Each extraction was done for 1800s in a 2-ml vial, at near boiling temperature for water (371 K), ethanol (349 K), chloroform (332 K), and acetone (327 K). The remaining CWR was dried under vacuum. The lignin composition is evaluated via thioacidolysis as described by Foster et al. [32]. The monomers involved in β-O-4-ether bonds, released upon thioacidolysis, are detected with Gas Chromatography (GC) as their trimethylsilyl (TMS) ether derivatives. The equipment consists of a Hewlett-Packard HP 6890 GC system (Agilent) coupled with a HP-5973 mass selective detector and a 30-m RTX5 ms 0.25-mm internal diameter capillary column. One-microliter injections were separated using helium as a carrier gas at $1.6 \cdot 10-8$ m3/s. Inlet and detector temperatures were set to 523 K, while the oven profile consisted of: initial temperature 403° K, hold 180 s, ramp temperature 0.05 $K \cdot s-1$ for 2400s to give a final temperature of 523 K, hold 300 s, cool. Table 1 shows the molecular percentage of Gu, Hy and Sy units in pine and poplar lignins.

2.2. Gas-Solid Vortex reactor unit

The unit used in this work is shown in Fig. 1. The non-reactive version was described in detail by Gonzalez-Quiroga et al. [18]. The focus here is on the main components required to carry out the fast pyrolysis experiments.

Table 1
Ultimate analysis, proximate analysis and composition of units of lignin [34] of biomass.

		Pine	Poplar
Ultimate analysis, wt. % dry basis	C	49.7[a] ± 0.3[b]	49.0[a] ± 0.3[b]
	H	6.31[a] ± 0.07[b]	6.26[a] ± 0.07[b]
	O	43.6[a] ± 0.3[b]	43.9[a] ± 0.4[b]
	N	0.067[a] ± 0.010[b]	0.13[a] ± 0.04[b]
Proximate analysis, wt. % dry basis	Moisture	10.5[a] ± 0.4[b]	8.2[a] ± 0.7[b]
	Volatile Matter	83.80[a] ± 0.2[b]	85.60[a] ± 0.5[b]
	Ash	0.40[a] ± 0.10[b]	0.70[a] ± 0.10[b]
	HHV, MJ kg^{-1} [27]	20.3	19.9
Lignin units composition, mol%	Hy	(3.84[a] ± 0.80[b])·10^{-3}	(5.99[a] ± 2.44[b])·10^{-4}
	Sy	1.01[a] ± 0.4[b]	61.5[a] ± 0.1[b]
	Gu	99.0[a] ± 0.4[b]	38.4[a] ± 0.1[b]

[a] Average of three measurements.
[b] Standard deviation of three measurements.

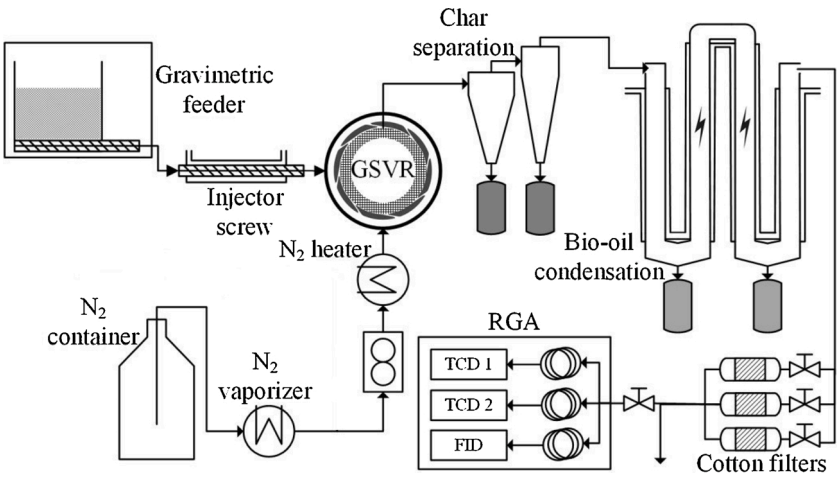

Fig. 1. Flow diagram of the Gas-Solid Vortex Reactor (GSVR) demonstration unit for biomass fast pyrolysis.

The N_2 supply and conditioning section consists of a liquid N_2 container connected to an electric vaporizer and an electric heater. The vaporized N_2 flows through an electric heater (Kanthal flow heater, Sandvik) in which the temperature can be increased up to 1265 K.

The biomass feeding section includes a gravimetric feeder (model KMLSFSKT20, Coperion K-Tron) equipped with a custom-made injector screw. The gravimetric feeder is enclosed in a gas leak-tight metallic tank, connected to vaporized N_2. The N_2 that flows through the biomass feeding section establishes an inert atmosphere and keeps pressure on the hopper. Silicon oil circulates through the injector screw jacket to prevent overheating of the particles and to avoid blockages due to thermal decomposition in the screw feeder.

Heated N_2 enters into the GSVR through the outer jacket and it is distributed in an 80 mm diameter reactive zone via 12 tangentially inclined rectangular slots, with a width of 060 mm. An absolute pressure sensor (Unik 5000, General Electric) with a span of 80–160 kPa is located on the outer wall of the gas inlet jacket. Three gauge pressure sensors measure the pressure at different positions inside the chamber, in a range from 0 to 35 kPa and with full-scale accuracy of ±0.04 %. Four thermocouples (type K, Thermo Electric Instrumentation) are located on the GSVR, as shown in Fig. 2, one in the gas inlet jacket and three inside the reactive chamber (in a similar layout to the pressure sensors). Fig. 2b illustrates the geometry of the GSVR used in this work. Data are acquired at a frequency of 10 Hz and processed using the IBA Analyzer 6.10.0 (IBA A.G) software tool.

The solids separation section consists of two electrically heated cyclones. A 50 mm diameter high-throughput cyclone is placed in series with an 80 mm diameter high-efficiency cyclone. A double-lock mechanism at the bottom of the cyclones allows verifying the accumulation of char and collecting it during the reactive tests.

The inlet gas line, the GSVR, and the cyclones are insulated. The insulation consists of alkaline earth silicate wool (Insulfrax® LTX™ Blanket), with a maximum working temperature of 1200 °C.

Bio-oil condenses in a double pipe heat exchanger folded as a double U. The gases exiting the cyclones enter tangentially to enhance the inner-tube convective heat transfer coefficient. Cooling water flows through the jacket of the first U. Silicon oil from a cooler (model Integral XT 550, Lauda) circulates through the jacket of the second U. The bio-oil condensation section incorporates a single-stage electrostatic precipitator (ESP) consisting of two copper electrodes connected to a 15 kV

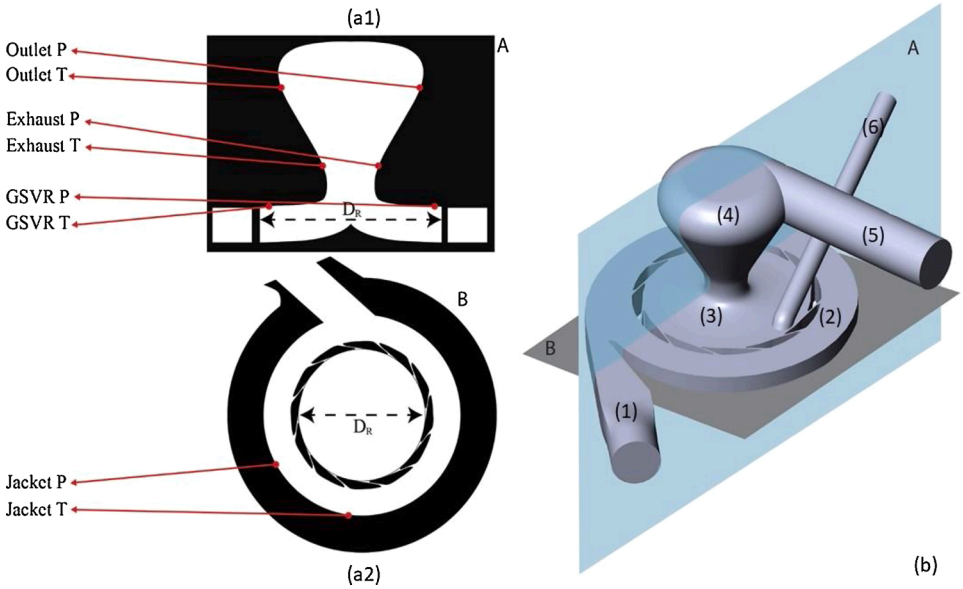

Fig. 2. Schematic representation of the GSVR: side view (a1) and top view (a2) showing the pressure sensors and thermocouple location. (b) 3D model of the GSVR, the cutting planes in the schematic representation are indicated. (1) Gas inlet, (2) gas distribution jacket, (3) reactor chamber, (4) diverging exhaust, (5) gas outlet, (6) custom-made injector screw for solid feeding.

power supply (model SPL-I-AC-15N50, HVP GmbH). An absolute pressure sensor with a span of 80–120 kPa is located in the bio-oil condensation section.

The non-condensable gases flow through cotton filters to the sampling section. Entrained bio-oil is removed by the filters to avoid plugging of the sampling lines. The composition of the non-condensable gases is quantified with an online refinery gas analyzer (RGA) (TraceGC 1310, Thermo Scientific), equipped with two thermal conductivity detectors (TCD) and a flame ionization detector (FID).

2.3. Experimental procedure

Before starting an experiment, the gas feeding section, the GSVR and the solid separation section are heated by hot gas until the temperature inside the reactor chamber is 15−20 K above the desired pyrolysis temperature (~773 K). The N2 mass flow rate is set at 5·10−3 kg·s-1. Two kg of biomass are initially stored in the gravimetric feeder. A N2 mass flow rate of 3.2·10−4 kg·s-1 is introduced at the biomass feeding section.

A typical fast pyrolysis experiment starts by feeding the cold biomass to the reactor using the screw feeder at a rate of 2.77·10−4 kg·s-1, resulting in an N2-to-biomass mass flow ratio of 19. Temperature and pressure values are continuously measured at several points (see Section 2.2) during the experiments. The transfer line and the cyclones are insulated and heated to avoid the condensation of the pyrolysis vapors, The bio oil condensation section is cooled in two stages, with tap water to 288 K and silicon oil to 243 K. The pyrolysis vapours condensate in the condensation section. The non-condensable gases pass through a set of cotton filters, to remove the fines, and are injected into the RGA. With the completion of the fast pyrolysis experiment, the yields of non-condensable gasses and char were determined by the method proposed by Van Geem et al. [33] and by weight of the char collected in the cyclones. The bio-oil yield was estimated by difference and was double checked by measuring the collected bio-oil obtained from the condensation section. The collected bio-oil is kept in a refrigerator at 283 K to prevent aging. Table 2 summarizes the experimental parameters of the pyrolysis experiments carried out in the GSVR.

2.4. Product analysis

The non-condensable gases are sampled and measured online with a refinery gas analyzer (TraceGC 1310, Thermo Scientific).

The carrier gas (i.e., N_2) also acts as an internal standard. The mass flow rate of CH_4 ($\dot{m}_{CH_4}$) present in the non-condensable fraction of the pyrolysis vapors is calculated from the known mass flowrate of internal standard $\dot{m}_{N_2}$ and the peak surface areas of N_2 and CH_4, as indicated in Eq. 1[33].

$$\dot{m}_{CH4} = \frac{f_{CH_4} \cdot A_{CH_4}}{f_{N_2} \cdot A_{N_2}} \dot{m}_{N_2} \quad (1)$$

f_{CH_4} and f_{N_2} are the respective response factors of CH_4 and N_2, while A_{CH_4} and A_{N_2} represent peak surface areas.

The response factor of CH_4 is chosen to be unity. The relative response factors of N_2, CO, CO_2, H_2, and all C4- compounds are determined using a well-defined calibration mixture (CRYSTAL, AirLiquide). CH_4 is used as the secondary internal standard. Mass flow rates of the permanent gases and other hydrocarbons are calculated as indicated in Eq. 2:

$$\dot{m}_i = \frac{f_i \cdot A_i}{f_{CH_4} \cdot A_{CH_4}} \dot{m}_{CH_4} \quad (2)$$

The mole fractions of all gas components and the amount of non-condensable fraction of the pyrolysis vapors are calculated from the corresponding mass flowrates.

The elemental compositions of chars and bio-oils are determined in a Flash EA2000 (Interscience, Belgium) equipped with a thermal conductivity detector (TCD) detector.

The bio-oil analysis is carried out using two ThermoScientific TRACE GC × GCs (Rtx-1 PONA x BPX-50, Interscience). Both devices are equipped with a dual-stage cryogenic CO2 modulator. Two different detectors are mounted on the GC × GCs, a flame ionization detector (FID) and a time-of-flight mass spectrometer (TOF-MS). A programmed temperature vaporization (PTV) injector is used for the FID analysis to avoid component discrimination during the injection. For the TOF-MS analysis, a split/splitless (SSL) injector is used because the component discrimination does not affect the results. Table 3 summarizes the settings of the GCxGCs (similar settings are used for the TOF-MS).

Data acquisition and processing are carried out using Thermo Scientific's Chrom-Card data system for the FID and Thermo Scientific's XCalibur software for the TOF-MS. The raw GC × GC-FID data files are exported as computable document format (CDF) files and imported into GC Image software (Zoex Corporation). With the aid of the GC Image software, the contour plotting, retention time measurement, peak fitting and blob integration are performed. The combined information from the chromatogram obtained in the GC × GC-FID and the National Institute of Standards and Technology (NIST) library MS confirmation are used for the tentative identification of the peaks.

The water content in the bio-oil fractions is determined by Karl Fischer titration.

3. Results

3.1. Operability and stability assessment of GSVR for pyrolysis

Accurate temperature control in the reactor is one of the desired features for the biomass fast pyrolysis reactor. A precise pyrolysis temperature maximizes the bio-oil yields with consistent chemical composition and ensures data reproducibility. Accurate temperature control was also identified as one of the main challenges for the pyrolysis of biomass to obtain reliable estimates of heat transfer rates [14,34].

In this work, the pyrolysis temperatures were controlled as accurately as possible. In classical FBs the axial and radial temperature differences typically exceed 15 K [35] in addition to local temperature differences due to the presence of gas bubbles [36]. Fig. 3 shows the temperature during the first fifteen minutes and the last ten minutes of a typical one-hour length experiment in the GSVR. The drop of

Table 2
Summary of the experimental operating conditions.

Parameter	Value
N_2 temperature at heater inlet	298 K
N_2 temperature at heater outlet	873 K
Biomass injection temperature	298 K
Average reactor temperature	773 K
Cyclones temperature	773 K
Total N_2 mass flow rate	$5.32 \cdot 10^{-3}$ kg·s^{-1}
Biomass mass flow rate	$2.77 \cdot 10^{-4}$ kg·s^{-1}
N_2 to biomass ratio	19.02
Water condenser temperature (first U condensation section)	288 K
Silicon oil condenser temperature (second U condensation section)	243 K

Table 3
GCxGC parameters used to analyze the bio-oil.

Detector	FID, 573 K, range of 10 %
Injection	Autosampler + PTV, 0.5 μL and 5·10−7 m^3/s split flow
First column	Rtx-1 PONA 50 m x0.25 mm I.D. × 0.5 μm df
Second column	BPX-50 2 m x0.15 mm I.D. × 0.15 μm df
Oven temperature	233 K→ 573 K at 5˙10−2 K/s
Modulation period	7 s, delay of 1080 s
Carrier gas	He, constant flow (3.5˙10^{-7} m^3/s)

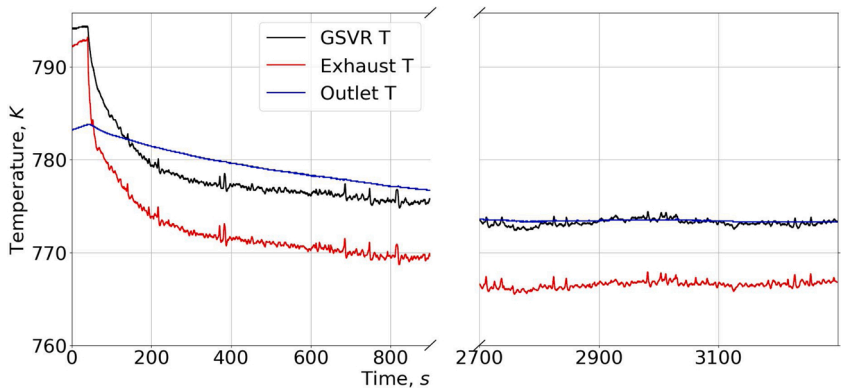

Fig. 3. Temperatures measured by thermocouples indicated in Fig. 2, during the start up and at the end of one typical fast pyrolysis experiment (time 0 correspond to the onset of cold biomass feeding).

temperature at the onset of reaction is a consequence of feeding cold biomass and the N_2 used to pressurize the biomass feeder. The temperature stabilized, with an average temperature in the reactor of 772 ± 3 K for almost an hour.

The high-speed hot gas injection ensures fast heating of the cold biomass particles. The minor fluctuations in the solid bed temperature could be attributed to the fluctuations in solids azimuthal and radial velocity. Note that the biomass and N_2 feeding accuracy, estimated as the relative standard deviation relying on the values taken over 60 s intervals, fall within 3 %.

The pressure stability during the pyrolysis of biomass is also remarkable. When the biomass feeding started, the differential pressure between the gas jacket and the reactor outlet ("Jacket P" and "Outlet P") dropped abruptly from 22 kPa to 11 kPa (Fig. 4). This reduction in the differential pressure is caused by suppression of primary and secondary flow phenomena (counterflow and backflow) when solids are introduced in the vortex chamber [22]. Once the biomass particles were rotating in the reactor, the differential pressure remained constant at a low value of approximately 11 kPa. This is an indication that the reactor was operating at a steady state with a steady amount of solids inside the chamber. During the experiments, the formed char was continuously removed by entrainment with the gas, and the cyclones downstream separated the solids from the gas. The fluctuations observed in Fig. 4 are a consequence of the GSVR solid loading due to the entrainment of the char.

3.2. Product fraction comparison

The pyrolysis products have been grouped into three different fractions: gas, bio-oil, and char.

The yields of each fraction are presented in Table 4.

As can be observed, there is no apparent difference in bio-oil nor non-condensable gases yields between pine and poplar pyrolysis. The average yield of the char produced in the pyrolysis of pine is higher than that of poplar (13.9 vs. 10.7 wt. %). It has been reported that lignins with a high content of syringyl units (methoxy groups), like poplar, produce less char during the fast pyrolysis process [37]. In both cases the bio-oil water content is consistent with a low yield of pyrolytic water. The higher average water content of pine bio-oil compared to that of poplar bio-oil can be explained by the higher humidity of the feedstock (10.5 vs 8.2 wt. %) and the dehydration reactions to form anhydrosugars starting from hemicelluloses from softwood [38].

The bio oil-yields obtained by pine fast pyrolysis in FBs are in the range of 61−68 wt. % on dry basis [39–42], with the average yield obtained in this work being 70 wt. % on dry basis. The pine biomasses used for the fast pyrolysis in FBs were similar to the pine biomass used in this work. The average char yield obtained in the GSVR is 13.9 wt. %, this value remains within the range of the values in the literature, 9.7–15.7 wt. % [39–42]. The average non-condensable gases yield in the GSVR was lower than those reported in the literature, 15.7 vs. 19–23.6 wt. % [39–42].

Table 4
Products (bio-oil, char, non-condensable gases and water) distribution.

wt. % dry basis	Pine	Poplar
Bio-oil	70.4	72.5
Char	13.9	10.7
Non-condensable gases	15.7	16.8
Water content of bio-oil	14.8	9.0

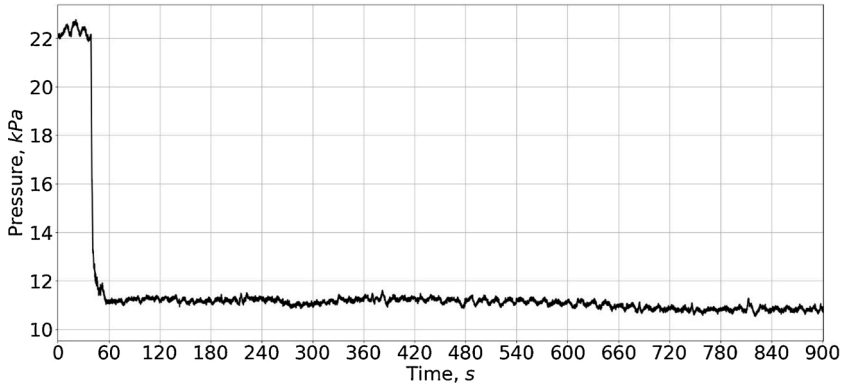

Fig. 4. Differential pressure profile across the reactor (difference between "Jacket P" and "Outlet P" pressure transducers) during the first 15 min of one of the fast pyrolysis experiments (time 0 correspond to the onset of cold biomass feeding).

Reported bio-oil yields for the fast pyrolysis of poplar in conventional FB reactors were lower than those obtained in the GSVR, at similar pyrolysis temperatures. The bio-oil yields for poplar were in the range of 60.9–68.5 wt. % [43–45], while the average bio-oil yield obtained in this work is 72.5 wt. %. The yields of char in the GSVR fall within the range of the char yields in conventional FB reactors [43–45]. Additionally, the reported char yields were consistently lower for poplar compared with pine, which is also the case for the GSVR. The average non-condensable gases yield in the GSVR is in the lower range of those in the literature, 16.8 vs. 14.3–24 wt. % [43–45]. The most substantial differences between conventional FB reactors and the GSVR are the low gas residence time in the GSVR and the selective entrainment of the char.

The low gas yields are an indication that gas-phase cracking reactions are suppressed due to the short gas residence time of the hot pyrolysis vapors in the GSVR. The elapsed time between the entrainment of pyrolysis vapors from the biomass particle and their condensation was in the order of 5–50 ms in the GSVR, while in conventional FBs it exceeded 0.5 s [35–38].

The continuous selective entrainment of the produced char limits the contact time of this with the hot pyrolysis vapors. The char is catalytically active promoting the cracking of the bio-oil to produce non-condensable gases [26].

These two phenomena lead to lower non-condensable and higher bio-oil yields obtained in fast pyrolysis in the GSVR compared to pyrolysis in conventional FBs.

Fig. 5 illustrates, in detail, the above-mentioned product yield distributions for the fast pyrolysis of both feedstocks in the GSVR. These are compared with the results of experiments carried out in conventional FB's [39–45]. The higher bio-oil yields in the GSVR are evident from the results, pointing the potential of GSVR for biomass fast pyrolysis.

3.3. Non-condensable gases and char composition

CO_2, CO, and CH_4 account for more than 96.5 mol % of the N_2-free non-condensable gases from the fast pyrolysis of pine and poplar in the GSVR. This was anticipated, as decarbonylation and decarboxylation are the predominant reactions in fast pyrolysis [46]. Other gases found in minor amounts are C_2H_6, C_2H_4, and H_2. Table 5 shows the composition of the non-condensable gases.

The non-condensable gases from fast pyrolysis in the GSVR are composed of a relatively high fraction of CO_2 and a low fraction of CH_4. The molar ratio CO/CO_2 from pine fast pyrolysis is 0.42 for the GSVR, while it ranged from 1.16 [39] to 1.28 [42] in conventional FBs. For poplar, the difference in the molar CO/CO_2 ratio is less marked, 0.39 for the GSVR vs. 0.73 for conventional FB [44]. It has been documented that hardwoods produce more CO_2 than softwoods, and the results from this work were in line with these findings [47]. High yields of CO and light hydrocarbons have been associated with the increased secondary cracking reactions of the pyrolysis vapors [46]. Fig. 6 shows the compositions of the non-condensable gases for the pyrolysis of pine and poplar in the GSVR and their comparison with the available data in literature.

Table 5
Non-condensable gases identified and quantified via RGA (N_2-free basis).

Analysis/parameter	Pine	Poplar
H_2, mol %	0.06[a] ± 0.01[b]	0.01[a] ± 0.01[b]
CO_2, mol %	65.65[a] ± 1.51[b]	71.22[a] ± 0.77[b]
CO, mol %	27.96[a] ± 7.4[b]	28.41[a] ± 0.86[b]
CH_4, mol %	2.97[a] ± 1.26[b]	0.23[a] ± 0.14[b]
C_2H_4, mol %	0.26[a] ± 0.09[b]	0.04[a] ± 0.01[b]
C_2H_6, mol%	0.76[a] ± 0.01[b]	0.10[a] ± 0.05[b]
Molar CO/CO_2 ratio	0.42	0.39

[a] Average of three measurements.
[b] Standard deviation of three measurements.

Consequently, the relatively high amount of CO_2 in the non-condensable gases in the GSVR provides a further indication of the suppression of secondary cracking of pyrolysis vapors due to rapid entrainment and condensation. This result opens perspectives for increasing the pyrolysis temperature to enhance selectivity towards bio-oil without excessive production of non-condensable gases. For example, Pyrolysis-gas chromatography-mass spectrometry (Py-GC/MS) experiments with poplar have shown that at high temperatures, the majority of lignin present in the biomass was volatilized into the bio-oil instead of remaining fixed in the char with the disadvantage of an increase in gas yield [48].

Table 6 shows the elemental compositions of the chars. Char from poplar presents higher nitrogen and ash content than the char from pine, which is consistent with the feedstock composition. A balance of elemental carbon shows that 21 % of C in pine and 15 % of C in poplar are present in the corresponding chars. The higher char yield formed in the pyrolysis of pine compared to that of poplar is the main reason for the difference in elemental C balance.

Compared to the feed (Table 1), char from pine is enriched in carbon, containing less hydrogen and oxygen. The elemental composition of the char obtained in the GSVR is similar to the composition of char obtained via the fast pyrolysis of pine in conventional FBs, as reported in the literature [13,39,49]. The low char yield can be attributed to the fast biomass heating rate in the GSVR and rapid entrainment of pyrolysis vapors [50].

The elemental composition of char from poplar fast pyrolysis in a conventional FB depends on pyrolysis temperature and residence time

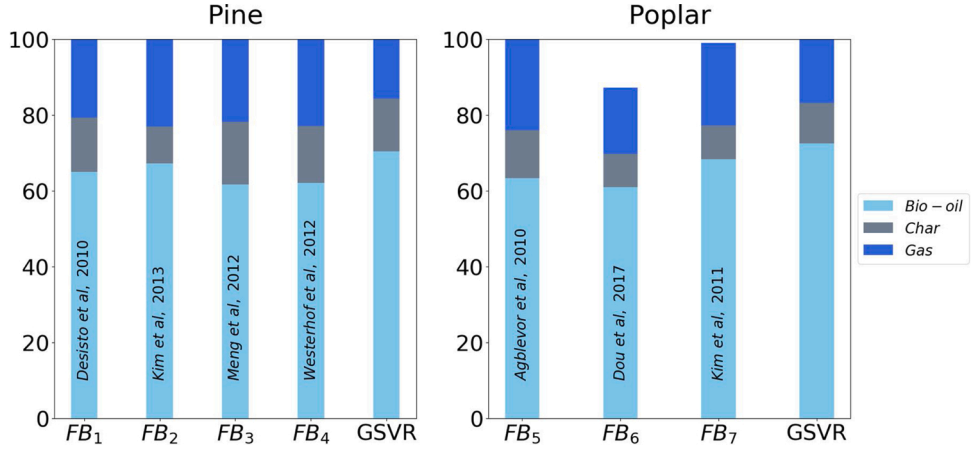

Fig. 5. Comparison of products yields on feed basis for the fast pyrolysis of pine and poplar in conventional FBs and in the GSVR. FB_1 [39], FB_2 [40], FB_3 [41], FB_4 [42], FB5 [43], FB_6 [44] and FB_7 [45].

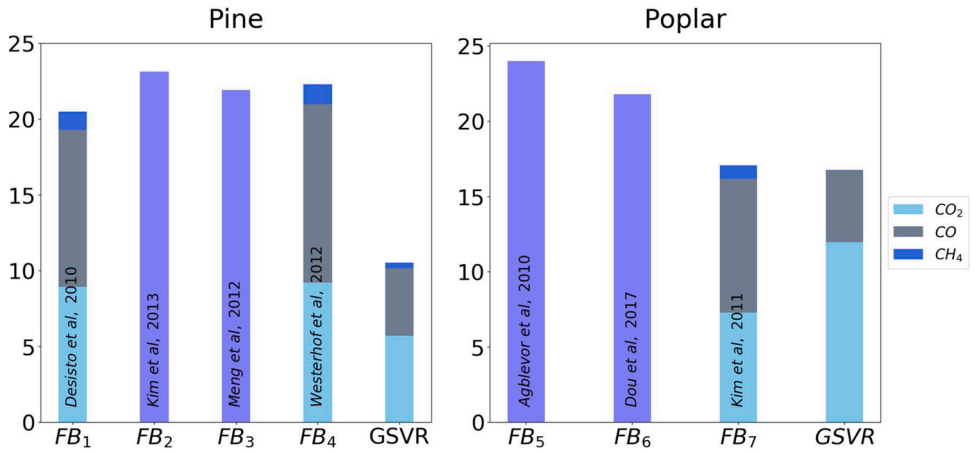

Fig. 6. Comparison of non-condensable gases yields on feed basis for the fast pyrolysis of pine and poplar in conventional FBs and in the GSVR. FB_1 [39], FB_2 [40], FB_3 [41], FB_4 [42], FB5 [43], FB_6 [44] and FB_7 [45].

Table 6
Char elemental compositions.

Analysis/parameter	Char from pine	Char from poplar
C, wt. %	73.6[a] ± 0.6[b]	73.3[a] ± 0.2[b]
H, wt. %	3.96[a] ± 0.19[b]	3.63[a] ± 0.01[b]
O, wt. %	20.6[a] ± 0.3[b]	20.9[a] ± 0.5[b]
N, wt. %	0.14[a] ± 0.01[b]	0.24[a] ± 0.01[b]
Ash, wt. %	1.70[a] ± 0.10[b]	1.90[a] ± 0.10[b]
molar H/C ratio	0.64	0.59
molar O/C ratio	0.21	0.21
HHV [27], MJ kg^{-1}	28.2	27.7

[a] Average of three measurements.
[b] Standard deviation of three measurements.

[45]. For a fixed pyrolysis temperature of 773 K, C content decreases with an increment of the residence time. H content follows the opposite trend. The elemental composition of the char in Table 5 is an indication of the short residence time compared with conventional FBs, which suggests differences in the molecular composition of char from the GSVR relative to those obtained from pyrolysis in conventional FBs.

3.4. Detailed bio-oil analysis

Although the main focus of this work was the study of the GSVR for biomass pyrolysis, with a special interest in obtaining a high yield of bio-oil predicted by the GSVR features, the GSVR has also its value to gain understanding of the kinetics because it allows to suppress secondary reactions [51,52].

Table 7 shows the bio-oil elemental compositions. Pine bio-oil exhibits lower C and higher H contents than poplar bio-oil, which is the first indication of molecular composition differences. The HHV is negatively affected by the oxygen content [27]. The higher O content in pine bio-oil results from the higher moisture content in the feedstock and dehydration reactions during the pyrolysis. An elemental balance indicates that 70 % of C in pine and 72 % of C in poplar are present in the corresponding bio-oils.

Table 7
Bio-oil elemental compositions.

Analysis/parameter	Pine	Poplar
C, wt. %	47.05[a] ± 1.15[b]	52.60[a] ± 1.70[b]
H, wt. %	7.09[a] ± 0.07[b]	6.67[a] ± 0.02[b]
O, wt. %	45.50[a] ± 1.10[b]	40.35[a] ± 1.75[b]
N, wt. %	0.11[a] ± 0.01[b]	0.12[a] ± 0.01[b]
molar H/C ratio	1.81	1.52
molar O/C ratio	0.73	0.57
HHV [27], MJ kg^{-1}	20.1	22.5

[a] Average of three measurements.
[b] Standard deviation of three measurements.

GCxGC has been chosen for the characterization of the bio-oil due to the wide detector linearity range and the high resolution. This allows the identification and quantification of a large number of components [53,54] and to better differentiate between the yields of the primary and secondary products. The latter is crucial to explain the differences in yield based on mechanistic understanding of the pyrolysis chemistry.

An example of the obtained GC × GC-FID chromatogram for pine bio-oils is shown in Fig. 7. Compounds were tentatively identified by using the orthogonal separation of the GC × GC method, while the internal standard, *i.e.*, fluoranthene, was adequately separated from other compounds.

Table 8 lists the aromatic compounds identified and quantified in the pine bio-oil, sorted by decreasing concentrations. These compounds account for 3.68 wt. % of the total bio-oil. Monoaromatic compounds with a carbon number between C_7-C_{10} represent more than 90 wt. % of the quantified aromatic fraction in the bio-oil.

Table 1 showed that the aromatics units in pine lignin are predominantly guaiacyl units. Therefore, guaiacols are predicted to be the prevalent monoaromatics in the pine bio-oil. On the other hand, the composition of the bio-oil is highly dependent on the temperature. Previous experiments with pine in conventional FBs [46] have shown that in the temperature range of 648−748 K, guaiacols are the dominant monoaromatics. If the temperature increases (748−848 K), the guaiacols content in bio-oil decreases, while the opposite occurs to the concentration of non-methoxy phenols. These results can be explained by the increment of dealkylation and demethoxylation reactions of guaiacols with the temperature. At a pyrolysis temperature of 848 K, aromatic hydrocarbons are present in bio-oil. During the pine pyrolysis experiments in the GSVR, the temperature was accurately controlled around 773 K (± 6 K). Table 8 shows that 15 out of 27 identified aromatics from the bio-oil are guaiacols, representing 85.06 wt. % of the quantified aromatics. Other aromatics that could be quantified in the bio-oil are catechols and phenols, representing 9.77 and 5.17 wt. % of quantified aromatics. These results together with the mechanistic insights in the biomass fast pyrolysis [51,52] suggest a marked selectivity towards guaiacols in the GSVR, despite the relatively high pyrolysis temperature. The high abundance of 4-substituted guaiacols with unsaturated alkyl groups (i.e., 4-methylguaiacol, vanillin, isoeugenol and 4-vinylguaiacol) suggests fast entrainment and quenching of the pyrolysis vapors. During secondary cracking reactions, the unsaturated alkyl groups in the guaiacols side chains are expected to become saturated alkyl groups and non-substituted types (i.e., H) [55]. In the GSVR, at an operating temperature of 773 K, the catechols/guaiacols ratio is less than 0.11, and the

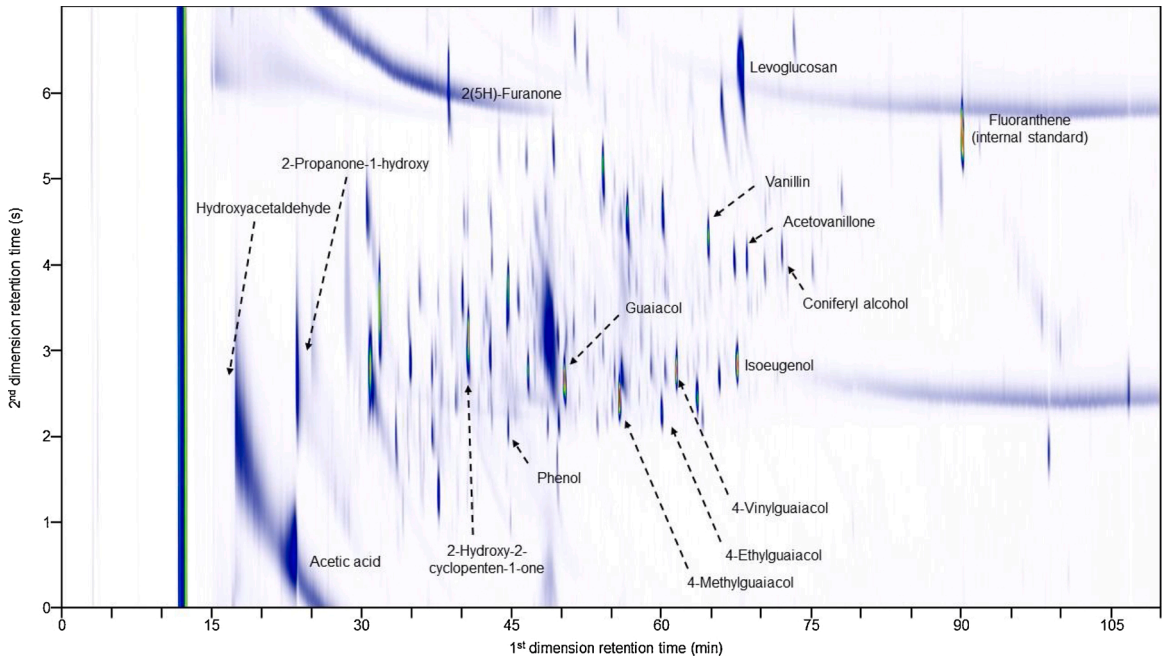

Fig. 7. GC × GC-FID chromatogram of pine bio-oil. Some representative compounds are pointed out.

Table 8
Aromatic compounds in pine bio-oil identified and quantified via GC × GC-FID/TOF-MS.

	Compound name	Concentration (wt. %)
1	2-Methoxy-4-methylphenol (4-methylguaiacol)[a]	0.54
2	2-Methoxyphenol (guaiacol)	0.45
3	4-Hydroxy-3-methoxybenzaldehyde (vanillin)	0.39
4	2-Methoxy-4-(1-propenyl)phenol (isoeugenol)	0.38
5	2-Methoxy-4-vinylphenol (4-vinylguaiacol)	0.26
6	1,2-Benzenediol (catechol)	0.19
7	1-(4-Hydroxy-3-methoxyphenyl)ethanone (acetovanillone)	0.19
8	4-Hydroxy-3-methoxyphenylethyl alcohol (homovanillyl alcohol)	0.17
9	2-Methoxy-3-(2-propenyl)phenol	0.16
10	4-Ethyl-2-methoxyphenol (4-ethylguaiacol)	0.12
11	4-(Ethoxymethyl)-2-methoxyphenol (vanillyl ethyl ether)	0.11
12	4-(3-Hydroxy-1-propenyl)-2-methoxyphenol (coniferyl alcohol)	0.11
13	3-Methyl-1,2-benzenediol (3-methylcatechol)	0.092
14	(Z)-2-Methoxy-4-(1-propenyl)phenol (cis-isoeugenol)	0.091
15	1-(4-Hydroxy-3-methoxyphenyl)-2-propanone (guaiacylacetone)	0.09
16	4-Methyl-1,2-benzenediol (4-methylcatechol)	0.073
17	3-Methylphenol (m-cresol)	0.049
18	Phenol	0.036
19	2-Methoxy-4-propylphenol (4-propylguaiacol)	0.03
20	4-Hydroxy-2-methoxycinnamaldehyde	0.03
21	2-Methylphenol (o-cresol)	0.025
22	2,3-Dimethylphenol	0.022
23	2-Methoxy-6-methylphenol	0.019
24	3-Methoxy-2-naphthalenol	0.013
25	4-Ethylphenol	0.012
26	2-Methoxy-6-(1-propenyl)phenol	0.012
27	3,4-Dimethoxytoluene	0.011
	Total	3.68

[a] Commonly use names for some compounds.

phenol/guaiacol ratio is 0.06. In a conventional FB, at 773 K, those ratios were 0.51 and 0.14 [39]. In an Auger reactor [56], the phenol/guaiacol and the catechol/guaiacol ratios were 2.12 and 5.03. The potential for improved selectivity towards guaiacols from the fast pyrolysis of softwoods in the GSVR is evident from those results. The main advantages of the GSVR over conventional fluidized bed reactors are the short residence time of the pyrolysis vapors, the entrainment of the char formed and the high heat/mass transfer rate.

Table 9 lists 29 non-aromatic compounds identified and quantified in pine bio-oil, sorted by decreasing concentrations. These compounds

Table 9
Non-aromatic compounds in pine bio-oil identified and quantified via GC × GC-FID/TOF-MS.

	Compound name	Concentration (wt. %)
1	Hydroxyacetaldehyde (glycolaldehyde)[a]	6.6
2	1,6-Anhydro-β-D-glucopyranose (levoglucosan)	5.19
3	Acetic acid	1.53
4	3,4-Altrosan	1.45
5	1-Hydroxy-2-propanone (acetol)	0.95
6	1,2-Ethanediol (ethylene glycol)	0.64
7	C6H10O5 (sugar)	0.54
8	5-(Hydroxymethyl)-2-furancarboxaldehyde (5-hydroxymethylfurfural)	0.44
9	5-Methyl-2(3 H)-furanone	0.42
10	2-Hydroxy-2-cyclopenten-1-one	0.4
11	5-(2-Propynyloxy)-2-pentanol	0.24
12	2-Hydroxy-3-methyl-2-cyclopenten-1-one	0.2
13	2,5-Dimethyl-4-hydroxy-3(2 H)-furanone	0.18
14	1,4:3,6-Dianhydro-α-D-glucopyranose	0.17
15	2-Furancarboxaldehyde (furfural)	0.16
16	3-Hydroxy-2-methyl-4H-Pyran-4-one (maltol)	0.088
17	3,4-Anhydro-D-galactosan	0.068
18	2,3-Dimethylfumaric acid	0.065
19	5-Acetoxymethyl-2-furaldehyde	0.064
20	2-Ethyl-1,3-dioxolane	0.059
21	7-methyl-1,4-Dioxaspiro[2.4]heptan-5-one	0.057
22	4-Methyl-2(5 H)-furanone	0.052
23	3-Methyl-1,2-cyclopentanedione	0.049
24	3-Methyl-2(5 H)-Furanone	0.046
25	6-Ethyltetrahydro-2H-pyran-2-one	0.046
26	5-Acetyldihydro-2(3 H)-furanone	0.04
27	5,6-Dihydro-2H-pyran-2-one	0.038
28	2-Cyclopentenone	0.03
29	Levoglucosenone	0.022
	Total	19.83

[a] Commonly used names for some compounds.

account for 19.8 wt. % of the bio-oil, with a carbon number in the range of C_2-C_8. Carbohydrates constitute two-thirds of the quantified non-aromatic hydrocarbons in the bio-oil. Glycolaldehyde and levoglucosan are the most abundant carbohydrates, with a concentration of 6.60 and 5.19 wt. % respectively. A high levoglucosan concentration has been reported for pine pyrolysis at 773 K using steam and N_2 as fluidization gas [57]. The use of steam as fluidization gas for pyrolysis in the GSVR is a plausible option to decrease the carrier-to-biomass ratio (for a pyrolysis temperature of 750 K, the heat capacity of the steam is twice as high as the N_2 capacity) while still providing the thermal energy for pyrolysis. Significant groups of non-aromatic compounds are the non-heterocyclic carboxylic acids, the ketones, and the alcohols, which sum for one-fourth of the mass of the quantified non-aromatics compound. Heterocyclic compounds, mostly furans, and pyrans, are also a considerable fraction of the pine bio-oil (8.5 wt. % of the quantified bio-oil).

A obtained GC × GC-FID chromatogram for poplar bio-oil is shown in Fig. 8.

In the case of the poplar bio-oil, 33 aromatic compounds have been tentatively identified and quantified. Table 10 lists the compounds according to their abundance. Those aromatic compounds consist of 4.21 wt. % of the poplar bio-oil. In contrast with pine bio-oil, compounds in the carbon range C_7-C_{10} account for only 65 % of the quantified aromatic fraction in poplar bio-oil, while C_6 compounds are more abundant.

Table 1 reveals that both Gu-type and Sy-type aromatics units are present in poplar lignin. Therefore, guaiacols and syringols are expected to be present in significant amounts in poplar bio-oil. The quantified bio-oil yields for pine and poplar are quite similar (≈ 70 wt. % dry basis); however, the concentration of aromatic monomers in the latter is on average ~15 % higher. The effect of temperature (573−1273 K) on the composition of the aromatic fraction of bio-oil from poplar has been studied in a Py–GC/MS setup [58]. Increasing the reaction temperature decreased the fraction of guaiacyls and syringyls compounds, while the amounts of catechols and phenols fractions increased [58]. These results can be explained by the promotion of demethoxylation, demethylation, and alkylation reactions to increase the phenolic, catechol-type, and cresol-type compounds while decreasing the Gu-type and Sy-type compounds, at higher temperatures [58]. Py-GC/MS experiments with lignins of Sy/Gu ratio (1.59–1.76) similar as in this work showed that the selectivity towards Gu-, Sy- and phenol-type monoaromatics was highly

Table 10
Aromatic compounds in poplar bio-oil identified and quantified via GC × GC-FID/TOF-MS.

	Compound name	Concentration (wt. %)
1	Phenol	0.78
2	2,6-Dimethoxyphenol (syringol)[b]	0.43
3	2-Methoxyphenol (guaiacol)	0.28
4	1,2-Dimethoxy-4-(2-methoxyethenyl)benzene	0.23
5	1-(3,5-dimethoxyphenyl)ethanone	0.23
6	1,2-Benzenediol (catechol)	0.2
7	4-Hydroxy-3-methoxybenzaldehyde (vanillin)	0.18
8	2-Methoxy-4-methylphenol (4-methylguaiacol)	0.15
9	2-Methoxy-4-(1-propenyl)phenol (isoeugenol)	0.14
10	2-Methoxy-4-vinylphenol (4-vinylguaiacol)	0.14
11	4-Methoxy-3-(methoxymethyl)phenol	0.14
12	3-Methoxy-1,2-benzenediol (3-methoxycatechol)	0.14
13	2,6-Dimethoxy-4-(2-propenyl)phenol	0.099
14	3-Methyl-1,2-benzenediol (3-methylcatechol)	0.094
15	4-Hydroxy-3,5-dimethoxybenzaldehyde (syringaldehyde)	0.092
16	4-Hydroxy-3-methoxyphenylethyl alcohol	0.091
17	2-Methoxy-3-(2-propenyl)phenol	0.077
18	1-(4-Hydroxy-3-methoxyphenyl)ethanone (acetovanillone)	0.075
19	3,5-Dimethoxy-4-hydroxycinnamaldehyde (sinapaldehyde)	0.065
20	4-Hydroxy-2-methocycinnamaldehyde	0.064
21	1-(2,4,6-Trihydroxyphenyl)-2-pentanone	0.063
22	4-Ethyl-2-methoxyphenol (4-ethylguaiacol)	0.057
23	4-(3-Hydroxy-1-propenyl)-2-methoxyphenol (coniferyl alcohol)	0.049
24	1-(4-Hydroxy-3-methoxyphenyl)-2-propanone	0.049
25	(Z)-2-Methoxy-4-(1-propenyl)phenol (cis-isoeugenol)	0.046
26	1,4-Benzenediol (hydroquinone)	0.045
27	3-Methylphenol (m-cresol)	0.041
28	4-Methyl-1,2-benzenediol (4-methylcatechol)	0.034
29	2,4-Dimethoxyphenol	0.031
30	1,2,3-Trimethoxy-5-methylbenzene	0.028
31	2-Methylphenol (o-cresol)	0.023
32	2,3-Dimethylphenol (o-xylenol)	0.016
33	2-Methoxy-4-propylphenol (4-propylguaiacol)	0.012
	Total	4.19

[b] Commonly used names for some compounds.

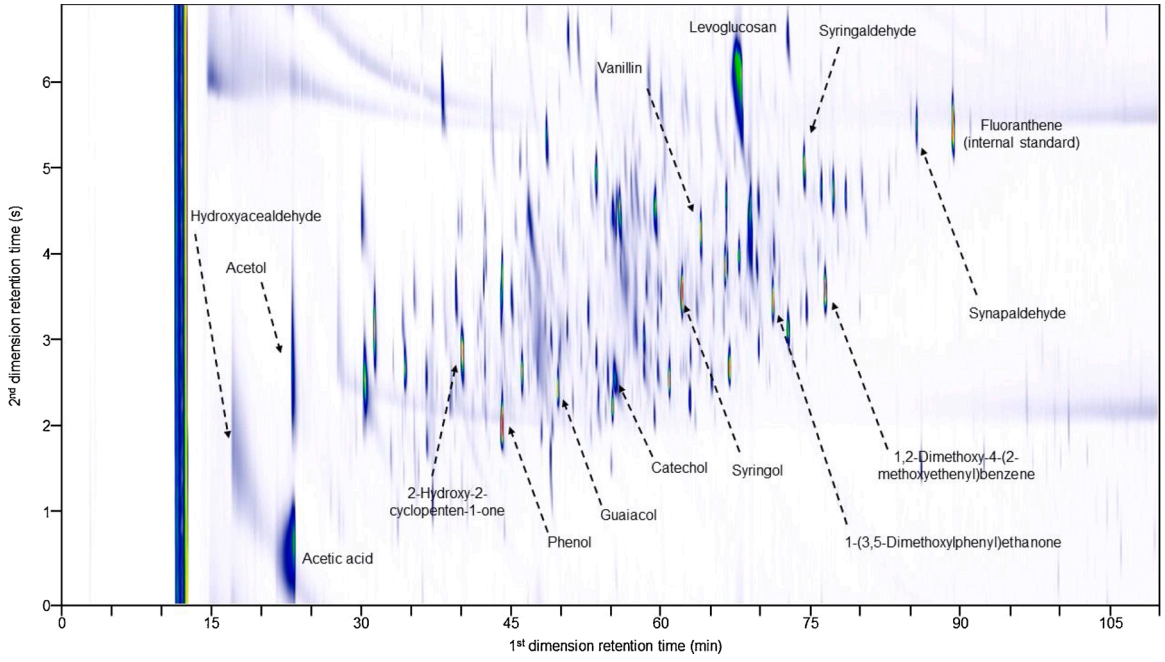

Fig. 8. GC × GC-FID chromatogram of poplar bio-oil. Some representative compounds are pointed out.

determined by reaction temperature [59]. The selectivity towards Sy-type compounds decreased continuously in the range 673−1073 K. The opposite behavior was observed for phenolics. In contrast, the selectivity towards Gu-type compounds peaked around 873 K [37,59]. Although results from "extracted" lignin and the feedstock are not directly comparable, it was proven that the selectivity towards specific groups of aromatic compounds could be enhanced via accurate control of the pyrolysis temperature together with fast condensation of pyrolysis vapors. These promising operation conditions can be reached in the GSVR.

A total of 14 out of 33 tentatively identified aromatics are guaiacols, and they account for approximately one-third of the mass of quantified aromatics in poplar bio-oil (Table 10). The most abundant mono-aromatic in poplar bio-oil is phenol, and nearly one-fourth of the quantified aromatics are phenolic-type compounds. After phenolics, syringol and catechols are the most abundant (16.2 and 11.2 wt. % of quantified aromatics). In contrast to pine bio-oil, in which guaiacyl compounds represent 85 wt. % of the quantified aromatics, poplar bio-oil has not shown a predominant aromatic group.

Three non-4-substituted compounds (i.e., -H at C_4) are the most abundant aromatics: phenol > syringol > guaiacol. For the rest of tentatively identified aromatics, most side-chains at the C_4 position are unsaturated alkyl groups, similar to what is found for aromatics in pine bio-oil. The mass ratio of tentatively identified Sy-/Gu-type compounds is 0.49, while the Sy/Gu lignin unit ratio is 1.6. These ratios suggest that Sy-type aromatic units in poplar underwent significant demethoxylation, which increased the concentration of Gu-type aromatics.

Table 11 lists 26 non-aromatic compounds that have been tentatively identified and quantified in poplar bio-oil, arranged in order of decreasing concentration. Those 26 compounds account for 22.6 wt. % of poplar bio-oil and exhibited carbon numbers in the range C_2-C_8. A similar carbon number range is also found for the non-aromatic compounds in pine bio-oil.

Carbohydrates account for approximately 50 % of the quantified non-aromatic oxygenates in poplar bio-oil. The concentration of glycolaldehyde in poplar bio-oil is higher than that in pine bio-oil; while the levoglucosan concentration was lower. Glycolaldehyde is a major product of hemicellulose fast pyrolysis [60], which differs significantly between softwoods and hardwoods. The concentration of non-heterocyclic oxygenates (mainly carboxylic acids, aldehydes, ketones, and alcohols) and heterocyclic oxygenates (mainly furans and pyrans) quantified in poplar bio-oil are comparable to those in pine bio-oil.

4. Conclusions

The main novelty of this work is twofold. The GSVR has been tested for the first time for reactive experiments at high temperature, and the potential of this reactor technology has been proved in the view of the results obtained, achieving high bio-oil yields, up to 72 wt. % at 773 K. Following the pressure drop over the bed in time, after feeding solids, confirmed that the unit reaches stable operation in around 60 s. Additionally, char is selectively removed while unconverted biomass is effectively retained based on the natural segregation based on particle sizes. Pyrolysis temperature can be controlled accurately, with small variations of the biomass temperature. Char yields for both pine and poplar in the GSVR are comparable to those in conventional FBs, while the yield of non-condensable gases is significantly lower. The latter is attributed to the effective suppression of secondary gas-phase cracking reactions mainly due to the well-defined and lower residence time of the pyrolysis vapors in the reactor. The differences in the bio-oil compositions obtained in the GSVR are an encouraging factor for using this technology for biomass fast pyrolysis. The results open perspectives to further intensify the process and to improve selectivity without excessive production of non-condensable gases.

Table 11
Non-aromatic compounds in poplar bio-oil identified and quantified via GC × GC-FID/TOF-MS.

	Compound name	Concentration (wt. %)
1	Hydroxyacetaldehyde (glycolaldehyde)[b]	7.48
2	1,6-Anhydro-β-D-glucopyranose (levoglucosan)	4.17
3	Acetic acid	3.13
4	1-Hydroxy-2-propanone (acetol)	1.89
5	Butanedial (Succinaldehyde)	0.93
6	2-Hydroxy-2-cyclopenten-1-one	0.89
7	2(3 H)-Furanone	0.71
8	Acetic acid ethenyl ester	0.67
9	2-Hydroxy-3-methyl-2-cyclopenten-1-one	0.37
10	2-Furanmethanol	0.35
11	2-Furancarboxaldehyde (furfural)	0.31
12	5-(Hydroxymethyl)-2-furancarboxaldehyde (5-hydroxymethylfurfural)	0.23
13	1,4:3,6-Dianhydro-α-D-glucopyranose	0.21
14	C6H10O5 sugar	0.2
15	2-(2-Butoxyethoxy)ethanol	0.15
16	5-(2-Propynyloxy)-2-pentanol	0.14
17	3,4-Altrosan	0.12
18	3,4-Anhydro-D-galactosan	0.11
19	3-Hydroxy-2-methyl-4H-Pyran-4-one (maltol)	0.1
20	2-Ethyl-1,3-dioxolane	0.091
21	3-Hydroxycyclohexanone	0.086
22	2-Cyclopentenone	0.073
23	Dihydro-6-methyl-2H-pyran-3(4 H)-one	0.063
24	2,3-Dimethylfumaric acid	0.06
25	6-Ethyltetrahydro-2H-pyran-2-one	0.055
26	5-Acetoxymethyl-2-furaldehyde	0.047
	Total	22.58

[b] Commonly used names for some compounds.

Author statement

Manuel Nunez Manzano: Validation, Formal analysis, Writing - Original Draft, Investigation.

Arturo Gonzalez Quiroga: Validation, Conceptualization, Writing - Original Draft, Investigation.

Patrice Perreault: Validation, Conceptualization; Formal analysis, Writing - Review & Editing, Investigation.

Sepehr Madanikashani: Formal analysis, Investigation.

Laurien A. Vandewalle: Validation, Conceptualization; Formal analysis, Writing - Review & Editing.

Guy B. Marin: Funding acquisition, Supervision, Writing - Review & Editing.

Geraldine J. Heynderickx: Funding acquisition, Supervision, Writing - Review & Editing

Kevin M. Van Geem: Funding acquisition, Project administration, Supervision, Conceptualization, Writing - Review & Editing.

Declaration of Competing Interest

The authors declare that they have no known competing financial interests or personal relationships that could have appeared to influence the work reported in this paper.

Acknowledgements

The SBO project "Bioleum" (IWT-SBO 130039) supported by the Institute for Promotion of Innovation through Science and Technology in Flanders (IWT) is acknowledged. The research leading to these results has also received funding from Ghent University through GOA project BOF16/GOA/004 (PRETREF). The research leading to these results has received funding from the European Research Council under the European Union's Seventh Framework Programme (FP7/2007-2013) / ERC grant agreement n° 290793 and from the European Research Council under the European Union's Horizon 2020 research and innovation

programme / ERC grant agreement n° 818607. Sepehr Madanikashani would like to acknowledge the support received from the European Regional Development Fund (ERDF) via the PSYCHE project (Interreg France-Wallonie-Vlaanderen) with co-financing from the provinces of East-Flanders and West-Flanders.

Appendix A. Supplementary data

Supplementary material related to this article can be found, in the online version, at doi:https://doi.org/10.1016/j.jaap.2021.105165.

References

[1] W. Stafford, W. De Lange, A. Nahman, V. Chunilall, P. Lekha, J. Andrew, J. Johakimu, B. Sithole, D. Trotter, Forestry biorefineries, Renew. Energy 154 (2020) 461–475.
[2] D. Mohan, C.U. Pittman, P.H. Steele, Pyrolysis of Wood/Biomass for bio-oil: a critical review, Energy Fuels 20 (2006) 848–889.
[3] S. Czernik, A.V. Bridgwater, Overview of applications of biomass fast pyrolysis oil, Energy Fuels 18 (2004) 590–598.
[4] F. Cheng, H. Bayat, U. Jena, C.E. Brewer, Impact of feedstock composition on pyrolysis of low-cost, protein- and lignin-rich biomass: a review, J. Anal. Appl. Pyrolysis 147 (2020), 104780.
[5] A.V. Bridgwater, Review of fast pyrolysis of biomass and product upgrading, Biomass Bioenergy 38 (2012) 68–94.
[6] L. Dai, N. Zhou, H. Li, W. Deng, Y. Cheng, Y. Wang, Y. Liu, K. Cobb, H. Lei, P. Chen, R. Ruan, Recent advances in improving lignocellulosic biomass-based bio-oil production, J. Anal. Appl. Pyrolysis 149 (2020), 104845.
[7] A.V. Bridgwater, D. Meier, D. Radlein, An overview of fast pyrolysis of biomass, Org. Geochem. 30 (1999) 1479–1493.
[8] R.E. Guedes, A.S. Luna, A.R. Torres, Operating parameters for bio-oil production in biomass pyrolysis: a review, J. Anal. Appl. Pyrolysis 129 (2018) 134–149.
[9] R. Aguado, M. Olazar, M.J. San José, G. Aguirre, J. Bilbao, Pyrolysis of sawdust in a conical spouted bed reactor. Yields and product composition, Ind. Eng. Chem. Res. 39 (2000) 1925–1933.
[10] S. Papari, K. Hawboldt, R. Helleur, Production and characterization of pyrolysis oil from sawmill residues in an auger reactor, Ind. Eng. Chem. Res. 56 (2017) 1920–1925.
[11] W.M. Lewandowski, K. Januszewicz, W. Kosakowski, Efficiency and proportions of waste tyre pyrolysis products depending on the reactor type—a review, J. Anal. Appl. Pyrolysis 140 (2019) 25–53.
[12] K.M. Qureshi, A.N. Kay Lup, S. Khan, F. Abnisa, W.M.A. Wan Daud, A technical review on semi-continuous and continuous pyrolysis process of biomass to bio-oil, J. Anal. Appl. Pyrolysis 131 (2018) 52–75.
[13] D. Howe, T. Westover, D. Carpenter, D. Santosa, R. Emerson, S. Deutch, A. Starace, I. Kutnyakov, C. Lukins, Field-to-Fuel performance testing of lignocellulosic feedstocks: an integrated study of the fast pyrolysis–hydrotreating pathway, Energy Fuels 29 (2015) 3188–3197.
[14] M.S. Mettler, D.G. Vlachos, P.J. Dauenhauer, Top ten fundamental challenges of biomass pyrolysis for biofuels, Energy Environ. Sci. 5 (2012) 7797–7809.
[15] G. Lopez, J. Alvarez, M. Amutio, B. Hooshdaran, M. Cortazar, M. Haghshenasfard, S.H. Hosseini, M. Olazar, Kinetic modeling and experimental validation of biomass fast pyrolysis in a conical spouted bed reactor, Chem. Eng. J. 373 (2019) 677–686.
[16] J. De Wilde, Gas–solid fluidized beds in vortex chambers, Chem. Eng. Process. Process. Intensif. 85 (2014) 256–290.
[17] J. De Wilde, A. de Broqueville, Rotating fluidized beds in a static geometry: experimental proof of concept, Aiche J. 53 (2007) 793–810.
[18] A. Gonzalez-Quiroga, P.A. Reyniers, S.R. Kulkarni, M.M. Torregrosa, P. Perreault, G.J. Heynderickx, K.M. Van Geem, G.B. Marin, Design and cold flow testing of a Gas-Solid Vortex reactor demonstration unit for biomass fast pyrolysis, Chem. Eng. J. 329 (2017) 198–210.
[19] R.P. Ekatpure, S. Vaishali, G. Heynderickx, A. de Broqueville, B. Marin, Experimental Investigation of a Gas–solid Rotating Bed Reactor With Static Geometry, 2011.
[20] R.W. Ashcraft, G.J. Heynderickx, G.B. Marin, Modeling fast biomass pyrolysis in a gas-solid vortex reactor, Chem. Eng. J. 207 (2012) 195–208.
[21] S. Kulkarni, L. Vandewalle, A. Quiroga, P. Perreault, G. Heynderickx, K. Marcel Van Geem, G.B. Marin, CFD-assisted Process Intensification Study for Biomass Fast Pyrolysis in a Gas-Solid Vortex Reactor, 2018.
[22] S.R. Kulkarni, A. Gonzalez-Quiroga, M. Nuñez, C. Schuerewegen, P. Perreault, C. Goel, G.J. Heynderickx, K.M. Van Geem, G.B. Marin, An experimental and numerical study of the suppression of jets, counterflow, and backflow in vortex units, AIChE J. 65 (2019), e16614.
[23] K. Niyogi, M.M. Torregrosa, M.N. Pantzali, G.J. Heynderickx, G.B. Marin, Experimentally validated numerical study of gas-solid vortex unit hydrodynamics, Powder Technol. 305 (2017) 794–808.
[24] L.A. Vandewalle, A. Gonzalez-Quiroga, P. Perreault, K.M. Van Geem, G.B. Marin, Process intensification in a gas–solid Vortex unit: computational fluid dynamics model based analysis and design, Ind. Eng. Chem. Res. 58 (2019) 12751–12765.
[25] S.R. Kulkarni, L.A. Vandewalle, A. Gonzalez-Quiroga, P. Perreault, G. J. Heynderickx, K.M. Van Geem, G.B. Marin, Computational fluid dynamics-assisted process intensification study for biomass fast pyrolysis in a gas–Solid Vortex reactor, Energy Fuels 32 (2018) 10169–10183.
[26] P. Gilbert, C. Ryu, V. Sharifi, J. Swithenbank, Tar reduction in pyrolysis vapours from biomass over a hot char bed, Bioresour. Technol. 100 (2009) 6045–6051.
[27] S.A. Channiwala, P.P. Parikh, A unified correlation for estimating HHV of solid, liquid and gaseous fuels, Fuel 81 (2002) 1051–1063.
[28] C. Álvarez, F.M. Reyes-Sosa, B. Díez, Enzymatic hydrolysis of biomass from wood, Microb. Biotechnol. 9 (2016) 149–156.
[29] M. Baucher, B. Monties, M.V. Montagu, W. Boerjan, Biosynthesis and genetic engineering of lignin, Crit. Rev. Plant Sci. 17 (1998) 125–197.
[30] W. Schutyser, T. Renders, S. Van den Bosch, S.F. Koelewijn, G.T. Beckham, B. F. Sels, Chemicals from lignin: an interplay of lignocellulose fractionation, depolymerisation, and upgrading, Chem. Soc. Rev. 47 (2018) 852–908.
[31] R. Van Acker, R. Vanholme, V. Storme, J.C. Mortimer, P. Dupree, W. Boerjan, Lignin biosynthesis perturbations affect secondary cell wall composition and saccharification yield in Arabidopsis thaliana, Biotechnol. Biofuels 6 (2013) 46.
[32] C.E. Foster, T.M. Martin, M. Pauly, Comprehensive compositional analysis of plant cell walls (Lignocellulosic biomass) part I: lignin, J. Vis. Exp. (2010) 1745.
[33] K.M. Van Geem, S.P. Pyl, M.-F. Reyniers, J. Vercammen, J. Beens, G.B. Marin, On-line analysis of complex hydrocarbon mixtures using comprehensive two-dimensional gas chromatography, J. Chromatogr. A 1217 (2010) 6623–6633.
[34] A.O. Kuzmin, M.K. Pravdina, A.I. Yavorsky, N.I. Yavorsky, V.N. Parmon, Vortex centrifugal bubbling reactor, Chem. Eng. J. 107 (2005) 55–62.
[35] G.S. Lee, S.D. Kim, Axial mixing of solids in turbulent fluidized beds, Chem. Eng. J. 44 (1990) 1–9.
[36] A.V. Patil, E.A.J.F. Peters, T. Kolkman, J.A.M. Kuipers, Modeling bubble heat transfer in gas–solid fluidized beds using DEM, Chem. Eng. Sci. 105 (2014) 121–131.
[37] S. Wang, G. Dai, H. Yang, Z. Luo, Lignocellulosic biomass pyrolysis mechanism: a state-of-the-art review, Prog. Energy Combust. Sci. 62 (2017) 33–86.
[38] S. Wang, B. Ru, H. Lin, W. Sun, Pyrolysis behaviors of four O-acetyl-preserved hemicelluloses isolated from hardwoods and softwoods, Fuel 150 (2015) 243–251.
[39] W.J. DeSisto, N. Hill, S.H. Beis, S. Mukkamala, J. Joseph, C. Baker, T.-H. Ong, E. A. Stemmler, M.C. Wheeler, B.G. Frederick, A. van Heiningen, Fast pyrolysis of pine sawdust in a fluidized-bed reactor, Energy Fuels 24 (2010) 2642–2651.
[40] K.H. Kim, T.-S. Kim, S.-M. Lee, D. Choi, H. Yeo, I.-G. Choi, J.W. Choi, Comparison of physicochemical features of biooils and biochars produced from various woody biomasses by fast pyrolysis, Renew. Energy 50 (2013) 188–195.
[41] J. Meng, J. Park, D. Tilotta, S. Park, The effect of torrefaction on the chemistry of fast-pyrolysis bio-oil, Bioresour. Technol. 111 (2012) 439–446.
[42] R.J.M. Westerhof, D.W.F. Brilman, W.P.M. van Swaaij, S.R.A. Kersten, Effect of temperature in fluidized bed fast pyrolysis of biomass: oil quality assessment in test units, Ind. Eng. Chem. Res. 49 (2010) 1160–1168.
[43] F.A. Agblevor, S. Beis, O. Mante, N. Abdoulmoumine, Fractional catalytic pyrolysis of hybrid poplar wood, Ind. Eng. Chem. Res. 49 (2010) 3533–3538.
[44] C. Dou, D.S. Chandler, F.L.P. Resende, R. Bura, Fast pyrolysis of short rotation coppice poplar: an investigation in thermochemical conversion of a realistic feedstock for the biorefinery, ACS Sustain. Chem. Eng. 5 (2017) 6746–6755.
[45] K.H. Kim, I.Y. Eom, S.M. Lee, D. Choi, H. Yeo, I.-G. Choi, J.W. Choi, Investigation of physicochemical properties of biooils produced from yellow poplar wood (Liriodendron tulipifera) at various temperatures and residence times, J. Anal. Appl. Pyrolysis 92 (2011) 2–9.
[46] Y.-M. Kim, J. Jae, S. Myung, B.H. Sung, J.-I. Dong, Y.-K. Park, Investigation into the lignin decomposition mechanism by analysis of the pyrolysis product of Pinus radiata, Bioresour. Technol. 219 (2016) 371–377.
[47] M. Asmadi, H. Kawamoto, S. Saka, Characteristics of softwood and hardwood pyrolysis in an ampoule reactor, J. Anal. Appl. Pyrolysis 124 (2017) 523–535.
[48] B. Klemetsrud, D. Eatherton, D. Shonnard, Effects of lignin content and temperature on the properties of hybrid poplar bio-oil, Char, and gas obtained by fast pyrolysis, Energy Fuels 31 (2017) 2879–2886.
[49] B.-S. Kang, K.H. Lee, H.J. Park, Y.-K. Park, J.-S. Kim, Fast pyrolysis of radiata pine in a bench scale plant with a fluidized bed: influence of a char separation system and reaction conditions on the production of bio-oil, J. Anal. Appl. Pyrolysis 76 (2006) 32–37.
[50] M. Somerville, A. Deev, The effect of heating rate, particle size and gas flow on the yield of charcoal during the pyrolysis of radiata pine wood, Renew. Energy 151 (2020) 419–425.
[51] A. Gonzalez-Quiroga, K.M. Van Geem, G.B. Marin, Towards first-principles based kinetic modeling of biomass fast pyrolysis, Biomass Convers. Biorefinery 7 (2017) 305–317.
[52] G. SriBala, H.-H. Carstensen, K.M. Van Geem, G.B. Marin, Measuring biomass fast pyrolysis kinetics: state of the art, WIREs Energy Environ. 8 (2019) e326.
[53] M.R. Djokic, T. Dijkmans, G. Yildiz, W. Prins, K.M. Van Geem, Quantitative analysis of crude and stabilized bio-oils by comprehensive two-dimensional gas-chromatography, J. Chromatogr. A 1257 (2012) 131–140.
[54] L. Negahdar, A. Gonzalez-Quiroga, D. Otyuskaya, H.E. Toraman, L. Liu, J.T.B. H. Jastrzebski, K.M. Van Geem, G.B. Marin, J.W. Thybaut, B.M. Weckhuysen, Characterization and Comparison of Fast Pyrolysis Bio-oils from Pinewood, Rapeseed Cake, and Wheat Straw Using 13C NMR and Comprehensive GC × GC, ACS Sustain. Chem. Eng. 4 (2016) 4974–4985.
[55] T. Hosoya, H. Kawamoto, S. Saka, Secondary reactions of lignin-derived primary tar components, J. Anal. Appl. Pyrolysis 83 (2008) 78–87.
[56] S. Thangalazhy-Gopakumar, S. Adhikari, H. Ravindran, R.B. Gupta, O. Fasina, M. Tu, S.D. Fernando, Physiochemical properties of bio-oil produced at various temperatures from pine wood using an auger reactor, Bioresour. Technol. 101 (2010) 8389–8395.

[57] E. Kantarelis, W. Yang, W. Blasiak, Production of liquid feedstock from biomass via steam pyrolysis in a fluidized bed reactor, Energy Fuels 27 (2013) 4748–4759.
[58] C.-q. Dong, Z.-f. Zhang, Q. Lu, Y.-p. Yang, Characteristics and mechanism study of analytical fast pyrolysis of poplar wood, Energy Convers. Manage. 57 (2012) 49–59.
[59] C. Liu, J. Hu, H. Zhang, R. Xiao, Thermal conversion of lignin to phenols: relevance between chemical structure and pyrolysis behaviors, Fuel 182 (2016) 864–870.
[60] X. Zhou, W. Li, R. Mabon, L.J. Broadbelt, A mechanistic model of fast pyrolysis of hemicellulose, Energy Environ. Sci. 11 (2018) 1240–1260.